Zhi-Yong Wu[1]
Fang Fang[1]
Jacques Josserand[2]
Hubert H Girault[2]

[1]Research Center of Analytical Science,
Northeastern University,
Shenyang, P. R. China
[2]Laboratoire d'Electrochimie Physique et Analytique,
Ecole Polytechnique Fédérale de Lausanne,
Lausanne, Switzerland

Received June 27, 2007
Revised August 4, 2007
Accepted August 8, 2007

Research Article

On-column conductivity detection in capillary-chip electrophoresis

On-column conductivity detection in capillary-chip electrophoresis was achieved by actively coupling the high electric field with two sensing electrodes connected to the main capillary channel through two side detection channels. The principle of this concept was demonstrated by using a glass chip with a separation channel incorporating two double-Ts. One double-T was used for sample introduction, and the other for detection. The two electrophoresis electrodes apply the high voltage and provide the current, and the two sensing electrodes connected to the separation channel through the second double-T and probe a potential difference. This potential difference is directly related to the local resistance or the conductivity of the solution defined by the two side channels on the main separation channel. A detection limit of 15 μM (600 ppb or 900 fg) was achieved for potassium ion in a 2 mM Tris-HCl buffer (pH 8.7) with a linear range of 2 orders of magnitude without any stacking. The proposed detection method avoids integrating the sensing electrodes directly within the separation channel and prevents any direct contact of the electrodes with the sample. The baseline signal can also be used for online monitoring of the electric field strength and electroosmosis mobility characterization in the separation channel.

Keywords:
Capillary-chip electrophoresis / Conductivity detection / Electric coupling / On-column detection
DOI 10.1002/elps.200700456

1 Introduction

Miniaturization of CE has been studied intensively during the past decade for the development of micro total analytical systems (micro-TAS) [1–4]. Different detection methods for capillary-chip electrophoresis are currently available, but very few can be used for field or point-of-care applications. Indubitably, MS is the most powerful technique for the analysis of complex mixtures and fluorescence detection is the most widely used thanks to its high sensitivity and selectivity. The use of small light source such as semiconductor diode laser and light-emitting diode (LED) made the detection system more compact [5]. Introduction of liquid core waveguides simplified the optics even further [6]. Electrochemical detection, on the other hand, is also a sensitive detection method that requires a less sophisticated instrumentation and that is very amenable to miniaturization and high throughput measurements. Different electrochemical detection methods have been proposed for CE, either amperometric or potentiometric with the electrodes being located either at the end of the column or directly in or on the column. In- or on-column methods are superior for maintaining the separation power of CE, and are easier to integrate for chip electrophoresis, as it is possible to integrate the detection electrodes during the microfabrication process [7, 8]. The electric coupling of the high voltage necessary for the electrophoretic separation and the low electric signals used for the electrochemical detection has been a major technological hurdle and has limited the wider development and applications of electrochemical detection. Conductivity detection was one of the main electrochemical detection methods investigated in micro-TAS [9–19]. Both for end-of-column and for in-column conductivity measurements, electric-coupling may cause polarization at the sensing electrodes, bubble generation, or damage to the detection circuit. Besides these methods where the electrodes are in direct galvanic contact, conductivity information in separation channels can also be sensed by contactless methods to avoid electric-coupling [20]. These contactless conductivity measurements can be carried out with simply two electrodes, though the dynamic range could be improved by using a 4-electrode configuration [17].

Another way to avoid electric-coupling problems is to use it to realize the detection. For example, Bai *et al.* [19] reported a passive conductivity detection method by integrating two

Correspondence: Professor Zhi-Yong Wu, Research Center of Analytical Science, Northeastern University, Shenyang 110004, P. R. China
E-mail: zywu@mail.edu.cn
Fax: +86-24-83676698

Abbreviation: DC, direct current

carbon paste electrodes in a separation channel, and the detection was achieved by measuring the potential difference between the two sensing electrodes in contact with the flowing solution. Potential gradient detection also takes advantage of the electrophoresis voltage, and detection is carried out by measuring the potential disturbance caused by the passage of a sample band of different conductivity [21–24]. A common feature of the above mentioned examples is to take advantage of the electric coupling to realize the detection. Based on this strategy, we present here a conductivity detection method with a glass chip electrophoresis system using two sensing electrodes connected to the separation channel *via* two side channels forming a double-T structure. The same detector can also be used for monitoring the electric-field strength in the separation channel or to characterize the electro-osmostic mobility. A 15 μM K^+ detection limit was achieved without any optimization.

2 Materials and methods

2.1 Material and instrument

The 4-channel high-voltage source was home-made, each channel being independently controlled by PC computer in the range of −3 to +3 kV. Both output voltage and current can be indicated during operation. The voltage reader was also home-made with an input resistance of 10^{12} Ohm. One sensing electrode was connected to the signal input of the operational amplifier with independent battery power supply, and the other one to the relative ground. The output signal was isolated from the amplifier and filtered before connecting to a data acquisition card (12Bit DAQ PCI 1711 from Advantech, Taiwan), and digitized data were recorded by a LabView program (Ver 5.0, National Instruments).

The electrophoresis electrodes are made of a Pt wire of 0.8 mm in diameter and the sensing electrodes are made of an Ag/AgCl wire of 1.0 mm in diameter or a Pt wire of 0.8 mm in diameter. Running buffer was Tris-phosphate at pH 14;8.5 and Tris-HCl at pH 8.7. Deionized water was prepared with Water Pro PS system from Labconco Corporation. KCl and NaCl standard solutions were prepared with the same buffer solution as the BGE.

2.2 Electrophoresis chip

The chip with a two double-T layout is schematically shown in Fig. 1. One double-T was used for sample introduction, and the other for detection. The chip was fabricated by photolithography and wet etching, following procedures reported earlier [25]. After etching of the microstructure, access holes of about 1 mm diameter were machined using a diamond drill. The chip was then cleaned, hydrolyzed, and put together with the cover under running water for sealing. The chip was left overnight under ambient conditions, and heated gradually up to 500°C in 3 h, and maintained for another 3 h and then cooled naturally to room temperature. Top width of the channel was 110 μm, depth 35 μm, total length 53 mm, and effective length 45 mm (central distance between the two double-Ts). Distance between the detection cell defined by the two side detection channels and the outlet reservoir of the separation channel was about 500 μm. The geometric features were characterized by a optical microscopy with a scalar of minimum nomination of 10 μm. Two sensing electrodes (RE1 and RE2) were placed directly in the outlet reservoirs of the detection side channels.

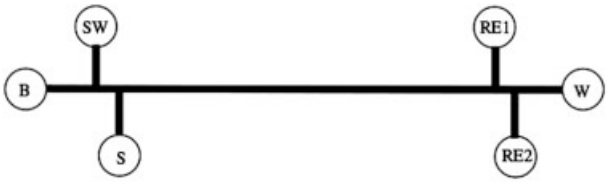

Figure 1. Layout of the chip. B, running buffer; S, sample; SW, sample waste; W, waste, RE1, RE2, sensing electrodes. The feed electrodes are placed in the B and W reservoirs.

2.3 Electrophoresis procedure

The channel system was first filled with running buffer, and then the same volume (~40 μL) of buffer was added in each of the six reservoirs. The buffer solution in the sample reservoir was replaced with the same volume of sample solution. Electro-sample introduction was carried out by applying voltage 50 V at S, –100 V at SW, 50 V at RB and W for 30 s, and then 350 V at RB, 300 V at S and SW, and 0 V at W. The above program was automatically repeated and controlled by a PC program.

2.4 Principle of detection

Figure 2 schematically shows the conductivity detection system for capillary-chip electrophoresis and the equivalent circuit. For simplicity, in Fig. 2A, the side channels for sample introduction are omitted. Taking the whole separation channel as a conductivity detection cell, then the two electrodes applying the high voltage act as the outer feed electrodes generating the electrophoretic current in the separation channel, and the two sensing electrodes as inner electrodes. The whole separation channel can be viewed as a linear resistance, and a potential difference is established between the two side detection channels. This potential difference can be directly detected by the two sensing electrodes with a voltmeter, and is used to correlate the resistance or conductivity of the detection cell defined by the two side channels on the main channel. Since the detection cell can be at a potential different to that of the outlet of separation channel, a proper isolation should be included in the voltage reader to prevent from any electric damage to the recording system.

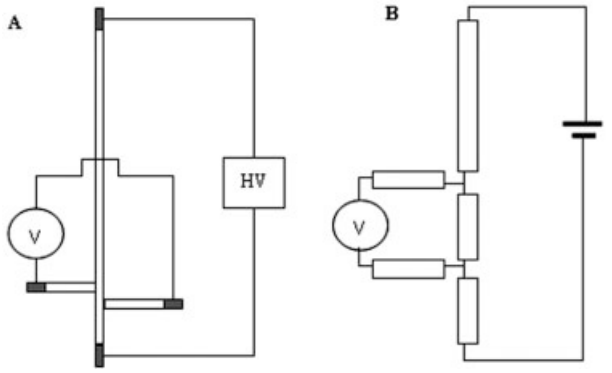

Figure 2. Principle of 4-electrode conductivity detection in CE (A) and the equivalent circuit (B).

2.5 Numerical model

A 2-D ohmic model is implemented on the finite element software Flux-Expert® (Astek) and operated on a Linux PC. The geometry is a vertical cross-section of the detection cell with the double-T. The Laplace Eq. (1) is solved:

$$\mathrm{div}\mathbf{j} = \mathrm{div}\left(-\sigma_{(x,t)}\mathrm{grad}\phi\right) = 0 \qquad (1)$$

where $\mathbf{j}$ is the electrical current density, ϕ the electrical potential, and $\sigma_{(x,t)}$ the solution conductivity associated to the presence of the buffer and a moving sample plug. To simulate the migrating sample, the electrical conductivity distribution $\sigma_{(x,t)}$ is taken as a linearly traveling Gaussian function added to the uniform buffer contribution σ_b:

$$\sigma_{(x,t)} = \sigma_b + \sigma_s^*(D, t_0)\exp\left(-\frac{(x-vt)^2}{4Dt_0}\right) \quad \text{for } t = t_0 \qquad (2)$$

where σ^*_s is the conductivity contribution given by the sample in addition to the buffer value σ_b, D the diffusion coefficient of the sample species under study, t_0 the electrophoresis time of the sample before the detection section, t the sample traveling time within the detection cell incorporating the double-T, and v the mean velocity of the sample plug, which represents the sum of both the electroosmotic and electrophoretic velocities. Diffusion as the plug is traveling through the double-T is neglected ($t_{detection} << t_0$). However, the band spreading by diffusion in the separating channel (4.5 cm) is taken into account by the terms $4Dt_0$ and σ^*_s/σ_b values in Eq. (2). σ_b is fixed to 1 and σ^*_s is normalized to 1 at the beginning of electrophoresis ($t_0 = 1$ s) for $D = 10^{-9}$ m^2/s. For the separation time here considered ($t_0 = 30$ s), a proportionality factor of $1/\sqrt{Dt_0}$ is applied to ensure that an equivalent amount of sample is always simulated for the different diffusion coefficient values. The electrical current density is imposed at the channel inlet to insure an electrical field of 100 V/cm. A zero potential value is defined at the end of the separating channel as a boundary condition. The detection channel simulated is 1 mm long, 100 μm wide with two side channels separated by 400 μm. A transient algorithm is used to calculate the evolution of the potential when the plug is moving through the geometry. A mesh size of 10 μm and a time step of 0.01 s are used for all the calculations.

3 Results and discussion

3.1 Numerical simulation

Figure 3 shows the variation of conductivity as a sample band passes through the double-T when the width of the Gaussian distribution is smaller than the length of the double-T.

Figure 4A shows the corresponding potential distribution in the double-T during the passage of the sample. It is important to notice that the potential is uniform within the two side channels showing that they act as Luggin capillaries. Figure 4B shows that the potential measured by the sensing electrode at the end of the side channel corresponds to the potential in the separation channel at a position that corresponds to the middle of the side channel, and that consequently the width of the side channel does not influence the response.

Figure 5 shows the electric field distribution and to a certain extent the EOF in the separation. It is interesting to notice that the presence of the side channel does not disturb significantly the electric field profile, and it can therefore be assumed that in turn the presence of the side channel does not perturb the sample plug migration through the double-T, causing additional band spreading. The main phenomenon that may induce perturbations of the sample plug is the diffusion in the side channels in the case of long sample plugs (high D values). However, this phenomenon is limited by the use of a sample velocity above 1 mm/s.

Figure 6 shows the detector response for different Gaussian distribution widths. Those widths are numerically obtained by varying the diffusion coefficient values in Eq. (2). We see that for a low diffusion coefficient ($D = 10^{-11}$ m^2/s)

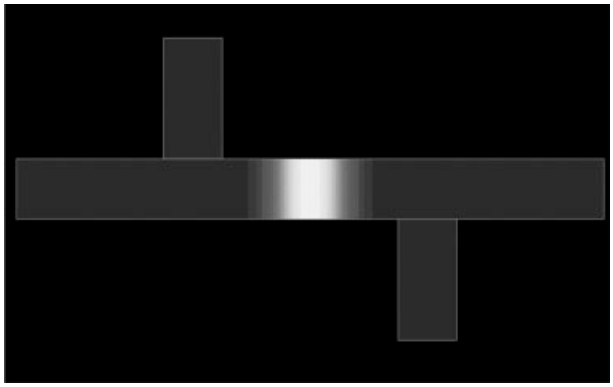

Figure 3. Conductivity variation during the passage of a sample of smaller length than the double-T ($D = 10^{-11}$ m^2/s). $t_0 = 30$ s, $t = 1$ s, $v = 1$ mm/s, σ_{peak}(yellow) = 1.183, σ_{min} (blue) = 1.

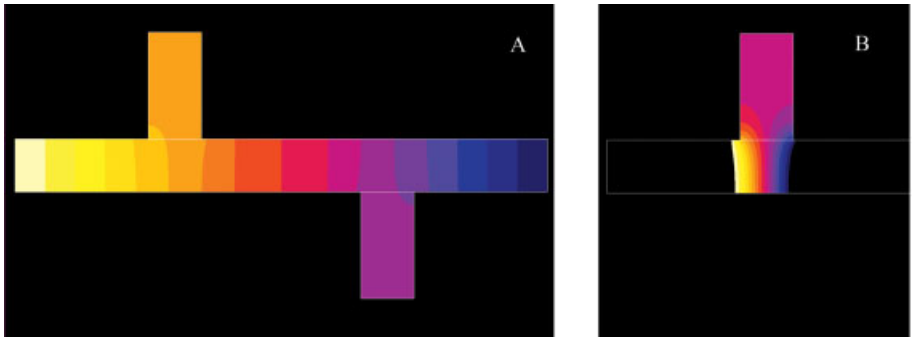

Figure 4. (A) Potential isovalues during the passage of the sample. The maximum value (yellow) corresponds to 9.47 V and the minimum one (blue) to 0 V. (B) Potential isovalues zoom at the junction of the side channel. The maximum value corresponds to 6.90 V and the minimum one to 5.9 V. The other parameters are those of Fig. 3.

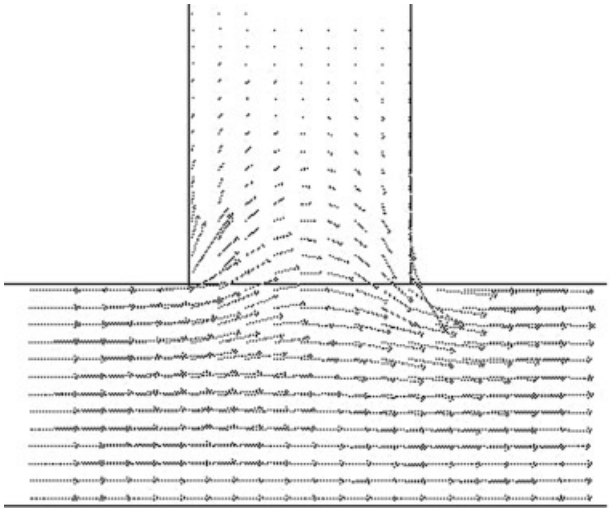

Figure 5. Electric field distribution at the junction of the side channel. The parameters are the same as for Fig. 3.

we have a Gaussian distribution thinner than the double-T (see Fig. 3) and therefore when this sample passes through the detector we observe a plateau response. Of course, this case is difficult to achieve experimentally in our case as we use also a double-T for injection, but the results is useful to benchmark this simulation study (*vide infra*). Inversely, when the Gaussian is larger than the double-T, the voltmeter yields also a bell shape response. The response of a Gaussian conductivity distribution of variance equal to $4Dt_0$ passing through the detector with a retention time t_R is given by the following equation:

$$\begin{aligned} R(t-t_R) &= \int_{-L/2}^{L/2} (\sigma_{(x,t)} - \sigma_b)dx = \\ &= \int_{-L/2}^{L/2} \sigma_s^* \exp\left(-\frac{(x-v(t-t_R))^2}{4Dt_0}\right)dx = \\ &= \sigma_s^*\left[-\sqrt{\pi Dt_0}\,\mathrm{erf}\left(-\frac{x-v(t-t_R)}{\sqrt{4\pi Dt_0}}\right)\right]_{-L/2}^{L/2} \approx \\ &\approx \sigma_s^* L \exp\left(-\frac{v^2(t-t_R)^2}{4Dt_0}\right) \end{aligned} \quad (3)$$

where L is the length of the separation channel across the voltage drop is measured, and can be considered as the distance between the center of the two side channels. This response approximates therefore to another Gaussian but a variance of $4Dt_0/v$. When the sample plug is much thinner than the double-T length, the differential conductivity response is then given by the following equation:

$$R(t-t_R) = \int_{-\infty}^{\infty} \sigma_s^*\left(-\frac{(x-v(t-t_R))^2}{4Dt_0}\right)dx = \sigma_s^*\sqrt{4\pi Dt_0} \quad (4)$$

Equation (4) corroborates the fact that the voltmeter response reaches a constant value in this case. The voltage response (plateau) can then be deduced from the Ohm's law using the sample contribution given by Eq. (4) to quantify the average conductivity value, $\overline{\sigma(t-t_R)} = \sigma_b + R(t-t_R)/L$ leading to

$$\Delta V_{plateau} = \frac{jL}{\overline{\sigma(t-t_R)}} = \frac{jL}{\sigma_b + \dfrac{\sigma_s^*\sqrt{4\pi Dt_0}}{L}} = \frac{\Delta V_{baseline}}{1+\sigma_s^*\sqrt{4\pi Dt_0}} \quad (5)$$

where σ_b is fixed to one. The term jL/σ_b corresponds to the 4 V theoretical baseline measured across L (here 400 μm). When the sample plug is larger than the double-T length, Eq. (5) becomes

$$\Delta V(t-t_R) = \frac{\Delta V_{baseline}}{1+\sigma_s^* L \exp\left(-\dfrac{\left(L/2 - v(t-t_R)^2\right)}{4Dt_0}\right)} \quad (6)$$

Equations (5) and (6) are in correct agreement with the simulated responses illustrated in Fig. 6b, when including the simulated baseline of 3.97 V instead of 4 V due to the enlargement of the current lines at the side channels levels (0.4% difference on the voltage "peak" between Eq. (5) and the case $D = 10^{-11}$ m^2/s and 2.9% difference between Eq. (6) and the case $D = 10^{-9}$ m^2/s). One can note that in the case $D = 10^{-9}$ m^2/s, the diffusion of the sample in the side channels should be taken into account to reach a perfect accuracy.

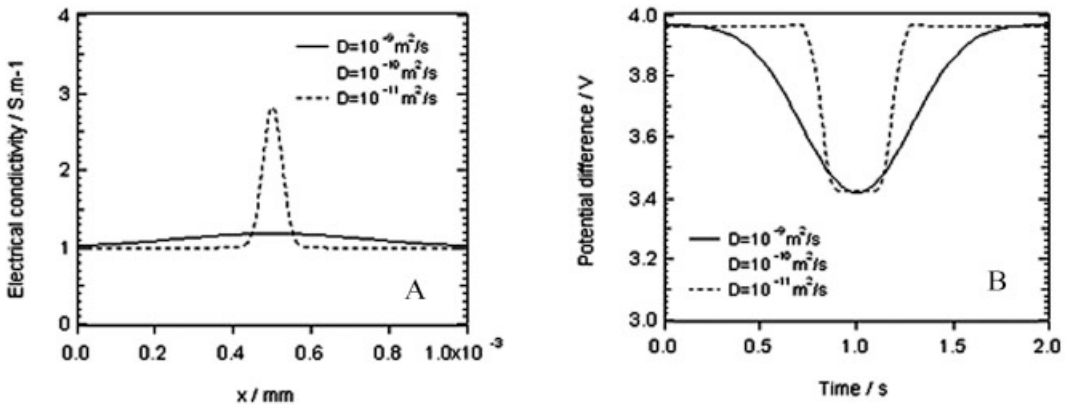

Figure 6. (a) Electrical conductivity distribution given by the sample plug in the presence of the buffer. (b) Time evolution of the voltage drop between the two side channels. L =400 μm, t_R = 1 s, v =1 mm/s.

3.2 Capillary chip electrophoresis with conductivity detection

Glass is a good chip substrate material optically transparent and with good electrical and surface properties, all very important in CE. However, integration of microelectrodes in the channel can be a technological challenge. Here, conductivity detection is achieved by measuring the potential difference with external macro reference electrodes placed in the reservoirs located at the extremity of the side detection channels. In this way, a reliable galvanic contact was achieved, and problems due to electrode poisoning [19] was avoided. This design is advantageous as it is easy to implement in term of microfabrication, as there is no limit to the choice of substrate material and as there is no restriction to the size of the sensing electrodes. Compared to a single electrode detection as used in ref. [24], the boundary of the detection cell is better defined, thus online monitoring of the electric field strength is also possible. More important is the fact that the sensing electrode is not used for applying the current, thus the detection accuracy is not influenced by electrolysis and polarization effects.

Direct current (DC) 4-electrode conductivity detectors have been used in ion chromatography to improve the detection range and to perform conductivity detection in high background conditions [26]. In this classical method, a constant DC current is applied between two outer feed electrodes, and conductivity detection is achieved by measuring the potential drop between two inner sensing electrodes. Because electrochemical reactions occur only on the outer electrodes, accurate conductivity detection can be made without interference due to sensing electrode polarization, capacitance effects, *etc.* Here, the two platinum feed electrodes (electrophoresis electrodes) provide the DC current flowing through the separation channel and the potential drop is measured across the double-T with the two sensing electrodes placed in the reservoirs located at the end of the two detection side channels. To make sure no current flows

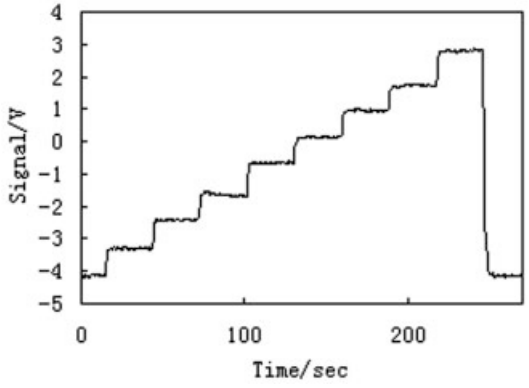

Figure 7. Potential difference signal response for a stepwise increase of the electrophoretic voltage by time.

in this detection loop, and the potential drop over the two side channels can be neglected, a voltage reader with high input impedance was used. Figure 7 is the potential difference measured as the applied voltage between the feed electrodes varies incrementally. As can be seen, the response is quite fast, and step increase to 90% of the step takes less than 0.5 s, this includes the time used for the high voltage source to generate a voltage step. The signal was offset to facilitate the recording as the potential drop can reach values up to 10 V depending the electrophoresis voltage and length of the detection cell. The potential–current ratio varies linearly with a variation coefficient better than 0.999, indicating the detection cell obeys Ohm's law with a resistance value of 472 kΩ. This test was made with the 252 μm detection cell, and a 50 mM Tris-H_3PO_4 buffer was used.

The sensing electrodes can be any types of electrode. We have used either simple silver/silver chloride electrodes or quasi reference platinum wires. As the current in the detection loop is negligible, no electrode polarization is involved, and as the two sensing electrodes are identical, the potential drop measured is zero when no current flows in the separa-

tion channel. Similar results were obtained with silver/silver chloride and platinum quasi reference electrodes.

As the potential difference measured across the double-T is due to electrical coupling, it should be independent to both buffer type and concentration. Figure 8 shows the influence of the buffer concentration, and it can be seen that all data fall on the same line with a combined linear coefficient better than 0.999. Tris-HCl and Tris-H_3PO_4 were also compared, and no major differences were found (data not shown). Higher voltages were not tried due to the range limit of the present voltage reader.

Figure 9 shows three consecutive injections of 5 mM K^+ and Na^+ in 10 mM Tris-HCl buffer. The first peak refers to K^+ and the second to Na^+ (76.2 and 51.9 $S \cdot cm^2 \cdot mol^{-1}$ respectively). Tris-ion (29.5 $S \cdot cm^2 \cdot mol^{-1}$) is less conductive, thus the two ions appeared as negative peaks. The third peak is the system peak associated to the EOF. The migration reproducibility was less than 0.5%, and that of peak height was 5%. As can be seen from the peaks profile, no obvious tailing is noticed, indicating that diffusion of solute band into the side detection channel is negligible. This is in agreement with the simulation analysis (Fig.5).

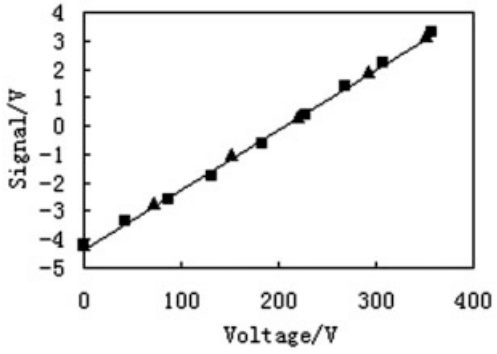

Figure 8. Comparison of 50 mM (triangle) and 10 mM Tris-H_3PO_4 (square), the line is a linear curve fitting of the combined dataset.

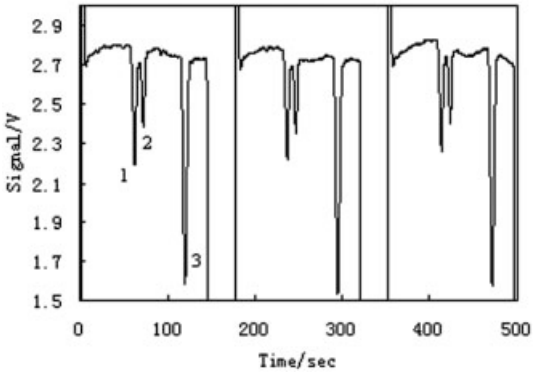

Figure 9. Electropherogram of three consecutive injections of a KCl and NaCl mixture, cell length 450 μm, sample: 5 mM KCl and NaCl in 10 mM Tris-HCl buffer, pH 8.7, electric field strength: 343 V over 5.3 cm.

Detection limit and linear range are two important aspects of a detector. According to theoretical analysis, an effective way to increase the method sensitivity is to increase the conductivity difference between the sample and the running buffer. Decreasing the buffer concentration is a practical method, but from an electrophoresis point of view, a certain concentration is necessary to maintain the buffer capacity. Figure 10 is the calibration curves of K^+ with different buffer concentrations, the sample being prepared in the running buffer solution. Below 2.5 mM, the calibration curves showed a linear coefficient better than 0.99 for both 2 and 10 mM buffer solutions. Five times dilution of the buffer resulted in sensitivity increase of about twice as estimated by the calibration slopes. The calibration curve was found to level off above 2.5 mM. With a 2 mM buffer concentration, the linear range was about 2 orders of magnitude from 0.03 to 2 mM.

As to the detection limit, dilution of running buffer from 10 to 2 mM resulted in a decrease of the detection limit from 0.15 to 0.015 mM (defined by S/N = 3). The detection limit was about 2 orders of magnitude lower than the concentration of the running buffer. And it was interesting to find that the absolute peak response was also comparable for different concentration levels maintaining the ratio of sample to buffer concentration (C_x/C_b), and as shown in Fig. 11 both for low and high sample concentrations. This indicates that by keeping the concentration ratio, or in other words by keeping the conductivity ratio (sample to buffer), the detection system can give similar absolute responses, which is in good agreement with the theoretical analysis. Molar conductivity could not be changed as a physical parameter, thus the conductivity ratio was changed by tuning the concentration ratio. This is meaningful since the detection limit can possibly be improved by decreasing the running buffer concentration. In conductivity detection, the noise level N is proportional to the background ΔV_b, $N = k_1 \Delta V_b$, k_1 is a system parameter which is of the order of 10^{-3} for the present system, and potentially can be improved to 10^{-6} [26]. Near the detection limit region, $C_b >> C_x$, the S/N ratio can be approximately expressed as:

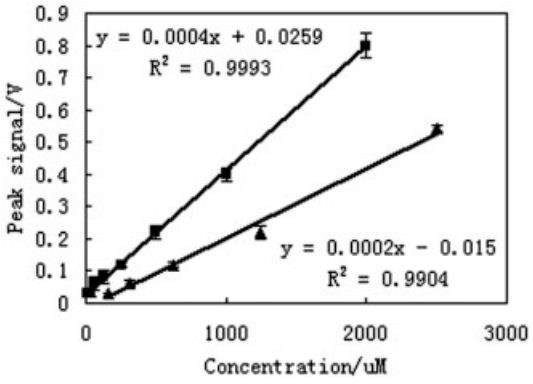

Figure 10. Calibration of K^+ with 2 mM (square) and 10 mM (triangle) pH 8.7 Tris-HCl buffer, each point is an average of four tests. Sample was introduced by pinched electric-injection.

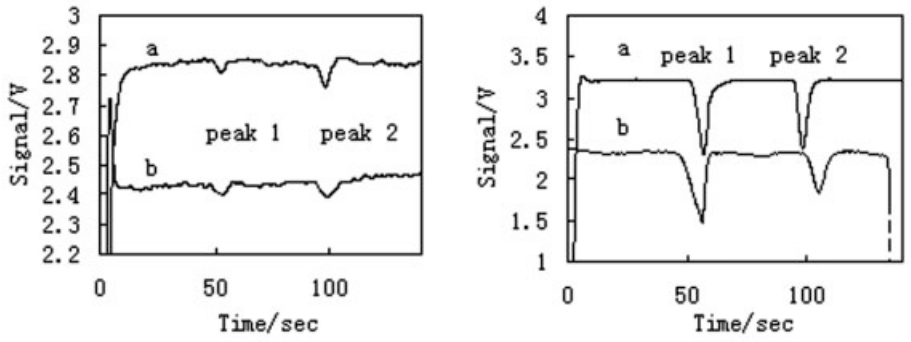

Figure 11. Electropherogram of 15 and 156 μM K^+ (left graph) and 2 and 10 mM K^+ (right graph) in 2 mM (curve a) and 10 mM (curve b) Tris-HCl, pH 8.7 respectively, peak 1 is K^+, and peak 2 the system peak.

$$\frac{S}{N} \approx \frac{1}{k_1} \cdot \frac{C_x \Lambda_x}{C_b \Lambda_b} \tag{7}$$

where Λ represents the molar conductivity. Therefore, the detection limit C_{Lim} defined by S/N = 3 can be estimated by $C_{Lim} \approx 3k_1 C_b \Lambda_b / \Lambda_x$, which indicates that high system stability (low k_1), low buffer concentration, and low mobility of buffer ions are beneficial for achieving a low concentration detection limit. For a 2 mM buffer, the estimated detection limit is about 0.005 mM. Experimental results are higher than this value because the sample is subjected to dilution during the electrophoresis process. In ion chromatography, very low detection limit at ppb (ng/mL) level can be reached by background depression. Introduction of background depression normally used in ion chromatography was also found effective in CE as demonstrated in the reports [27, 28].

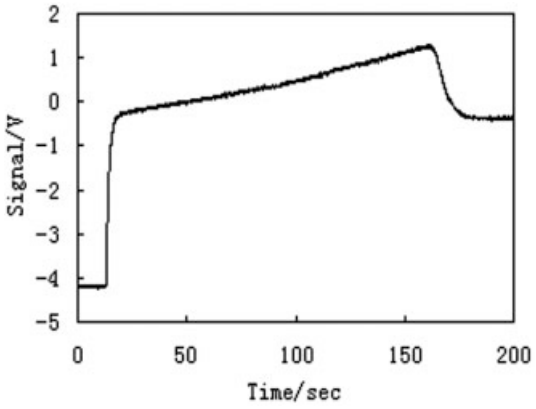

Figure 12. Substitution of a 5 mM buffer by a 10 mM buffer by EOF. Voltage was initiated at 15 s and held at 193 V during the test.

3.3 Electroosmotic mobility measurement

With the present detection method, chip electroosmotic mobility can be measured by monitoring the signal change associated to a step change of running buffer of different conductivity [29]. Before the interface between the two buffers reaches the detection cell, the cell contains only the original buffer and the solution resistance is therefore uniform. However, the potential drop along the separation channel changes gradually due to the variation of the current as the second buffer advances in the channel. This process was well observed as illustrated in Fig. 12 showing that the present setup can be used for EOF measurements. The channel was first filled with a 5 mM buffer, and was replaced with a 10 mM buffer by EOF pumping initiated by the application of the high voltage. Replacement of the low concentration buffer by the more concentrated one resulted in the decrease of the total resistance, yielding a current and signal increase. When the boundary passed the detection cell close to the end of the separation column, the signal becomes constant.

4 Concluding remarks

A DC conductivity detection was realized for CE as demonstrated by a glass chip electrophoresis system with a double T detection cell. The sensing electrodes were placed in the outlet reservoirs of the detection side channels constituting the double T. Conductivity detection was achieved measuring the potential difference between the two sensing electrodes, the signal being independent of the electrode material (supposing the two electrodes are the same and have stable contact potential in the buffer). The baseline level is defined by the electric field strength and cell length, and is independent of the buffer type and concentration as it is a fraction of the total voltage imposed. This potential difference fraction can also be used for the characterization of EOF in the same separation channel. Both numerical simulation and electrophoresis experiment results showed that sample diffusion into the side detections channels was not obvious with the present design.

The method is easy to implement, is not limited by chip material and difficulties of the electrode integration are also avoided. CE and conductivity are seamlessly incorporated comparing to the 4-electrode conductivity detection in IC where extra driving circuit is necessary, and interference from electrolysis product in the channel is prevented. Comparing to high frequency 4-electrode contactless conductivity detection, both chip fabrication and circuitry are much simplified. The character that S/N is independent of size and

concentration range is unique among detection methods, which is especially suitable for the development of highly integrated and portable lab on chip systems.

Further works include optimization of the detection cell structure, improvement in electrical stability, and working range of the circuit system, as well as its applicability in different electrophoresis modes and different types of solute. Portable chip electrophoresis with integrated universal conductivity detector and online monitoring of electric field strength is under development.

Financial supports from National Postdoc Foundation of China (2004036375), SRF for ROCS, SEM (200633105) and Northeastern University are acknowledged by one of the authors (Wu). The technical assistance of Valérie Devaud (EPFL) is also acknowledged.

5 References

[1] Manz, A., Graber, N., Widmer, H. M., *Sens. Actuators B* 1990, B1, 244–248.

[2] Manz, A., Harrison, D. J., Verpoorte, E. M. J., Fettinger, J. C. *et al.*, *J. Chromatogr.* 1992, *593*, 253–258.

[3] Harrison, D. J., Manz, A., Fan, Z., Ludi, H., Widmer, H. M., *Anal. Chem.* 1992, *64*, 1926–1932.

[4] Fang, Z. L., *Microfluidic Analytical Chip*, 1st Edn., Science Press, Beijing 2003.

[5] Renzi, R. F., Stamps, J., Horn, B. A., Ferko, S. *et al.*, *Anal. Chem.* 2005, *77*, 435–441.

[6] Wang, S. L., Huang, X. J., Fang, Z. L., Dasgupta, P. K., *Anal. Chem.* 2001, *73*, 4545–4549.

[7] Martin, R. S., Ratzlaff, K. L., Huynh, B. H., Lunte, S. M., *Anal. Chem.* 2002, *74*, 1136–1143.

[8] Chen, D. C., Hsu, F. L., Zhan, D. Z., Chen, C. H., *Anal. Chem.* 2001, *73*, 758–762.

[9] Manz, A., Miyahara, Y., Miura, J., Watanabe, Y. *et al.*, *Sens. Actuators B* 1990, B1, 249–255.

[10] Kappes, T., Hauser, P. C., *Electroanalysis* 2000, *12*, 165–170.

[11] Weber, G., Jöhnck, M., Siepe, D., Neyer, A., Hergenröder, R., in: Van den Berg, A., Olthuis, W., Bergveld, P. (Eds.), *Micro Total Analysis Systems 2000*, Kluwer Academic Publishers, Dordrecht 2000, pp. 383–386.

[12] Galloway, M. M., Soper, S. A., *Electrophoresis* 2002, *23*, 3760–3768.

[13] Galloway, M., Stryjewski, W., Henry, A., Ford, S. M. *et al.*, *Anal. Chem.* 2002, *74*, 2407–2415.

[14] Wang, J., Pumera, M., Collins, G. E., Mulchandani, A., *Anal. Chem.* 2002, *74*, 6121–6125.

[15] Pumera, M., Wang, J., Opekar, F., Jelinek, I. *et al.*, *Anal. Chem.* 2002, *74*, 1968–1971.

[16] Bodor, R., Kaniansky, D., Masar, M., Silleova, K., Stanislawski, B., *Electrophoresis* 2002, *23*, 3630–3637.

[17] Laugere, F., Guijt, R. M., Bastemeijer, J., Van der Steen, G. *et al.*, *Anal. Chem.* 2003, *75*, 306–312.

[18] Tanyanyiwa, J., Hauser, P. C., *Anal. Chem.* 2002, *74*, 6378–6382.

[19] Bai, X., Wu, Z., Josserand, J., Jensen, H. *et al.*, *Anal. Chem.* 2004, *76*, 3126–3131.

[20] Pungor, E., *Oscillometry and Conductometry*, Pergamon Press, Oxford 1965.

[21] Prest, J. E., Baldock, S. J., Bektas, N., Fielden, P. R. *et al.*, *J. Chromatogr. A* 1999, *836*, 59–65.

[22] Fukushi, K., Sagishima, K., Saito, K., Takeda, S. *et al.*, *Anal. Chim. Acta* 1999, *383*, 205–211.

[23] Qin, W., Li, S. F. Y., *J. Chromatogr. A* 2004, *1048*, 253–256.

[24] Feng, H. T., Wei, H. P., Li, S. F. Y., *Electrophoresis* 2004, *25*, 909–913.

[25] Yin, X., Shen, H., Fang, Z., *Ch. J. Anal. Chem.* 2003, *31*, 116–119.

[26] Jandik, P., Hadda, P. R., Stirrock, P. E., *Crit. Rev. Anal. Chem.* 1988, *20*, 1–74.

[27] Avdalovic, N., Pohl, C. A., Rocklin, R. D., Stillian, J. R., *Anal. Chem.* 1993, *65*, 1470–1475.

[28] Dasgupta, P. K., Bao, L., *Anal. Chem.* 1993, *65*, 1003–1011.

[29] Huang, X., Gordon, M. J., Zare, R. N., *Anal. Chem.* 1988, *60*, 1837–1838.

